Modulation of antichiral edge states in zigzag graphene nanoribbons by side potential

Jia-En Yang
Chongqing College of Electronic Engineering https://orcid.org/0000-0003-4682-1237
Xiao-Long Lü (physicslxl@163.com)
Guangxi University of Science and Technology
Hang Xie

Article

Keywords:

Posted Date: June 23rd, 2022

DOI: https://doi.org/10.21203/rs.3.rs-1732040/v1

Version of Record: A version of this preprint was published at Communications Physics on April 6th, 2023. See the published version at https://doi.org/10.1038/s42005-023-01183-3.

Abstract

Antichiral edge states induced by the modified Haldane model have been predicted by Colomés and Franz (Physical Review Letters, 2018, 120(8): 086603). By applying the side potential composed of a potential field, staggered electric field, and exchange field along the boundaries of zigzag graphene nanoribbons (zGNRs), we further propose other types of antichiral edge states and investigate their corresponding transport properties. It is found that the side potential could destroy one or two (spin) edge modes, eventually inducing five novel antichiral edge states. By calculating the effect of these external fields separately on the energy band of the zGNRs, the regulatory mechanism has been explained. In addition, based on these induced edge states, we also proposed the spin/charge switcher in the three-terminal device consisting of zGNRs. We believe that these results could be used for the future designs of spintronic devices.

1. Introduction

Graphene [1, 2], a 2D honeycomb crystal composed of carbon atoms, has attracted great attention since its many unconventional properties, such as the quantum Hall effect [3, 4], and the linear dispersion [5, 6]. Due to the linear dispersion near zero energy, the quantum Hall effect in graphene is characterized by chiral edge states [3]. Afterward, Kane and Mele [7, 8] predicted the quantum spin Hall (QSH) effect in graphene, which is characterized by helical edge states. Due to the importance of designing low-dissipation electronic devices [9–15], researchers are committed to finding more topological edge states.

Recently, Colomés and Franz [16] have theoretically proposed the antichiral edge state based on the modified Haldane model, where the edge states propagate in the same direction at two parallel boundaries and the bulk states propagate in opposite direction. Some possible schemes [17–21] for realizing the antichiral edge states have been proposed. For example, Hang et al. [20] construct an electrical circuit to realize a modified Haldane lattice with the antichiral edge states, which is of practical significance for theoretical applications. Based on the modified Haldane model, researchers propose the unipolar-bipolar filters [22], valley polarization [23], and topological phase transitions under uniaxial strain [24] in a honeycomb lattice. Besides, although the antichiral edge states are bulk gapless, which is robust against disorder [16] like the behavior of the QSH edge states. Thus, antichiral edge states have intriguing transport properties and potential applications in designing the low-dissipation spintronic device.

In previous literature, many methods have been used to manipulate the topological edge states. Xu et al. [25] proposed the anisotropic chiral edge modes by applying the circularly polarized light on the silicene. Marwa Mannaï et al. [24] have investigated the effect of the strain on the antichiral edge modes and found that the strain may reverse the direction of propagation of edge modes or eventually destroy them. Besides, the studies of graphene demonstrate that the side potential is an effective way to regulate the electronic structure [26–29]. Lu et al. [30, 31] studied the effect of the side potential on the QSH state edges of silicene, and they obtained various kinds of spin- and valley-related polarized edge states by

adjusting the side potential and ribbon width. However, the study of the side potential on the antichiral edge states of zigzag graphene ribbons (zGNRs) is still less considered.

In this paper, we investigate the side potential-tunable antichiral edge states in zGNRs with modified Haldane model. The schematic diagram of the considered side potential is shown in Fig. 1, and the side potential is composed of a potential field, staggered electric field, and exchange field applied on the boundaries of the zGNRs. We propose five types of antichiral edge states by modulating the side potential, which is important for designing the spin/charge switcher. Furthermore, we also explain the regulatory mechanism by calculating the effect of these external fields separately on the energy band of the zGNRs. In addition, taking one case of Type-3 as an example, we show that these induced antichiral edge states have potential application in the spin/charge switcher designs.

2. Model And Methods

The antichiral edge states can be obtained based on the modified Haldane model in zGNRs. Considering the side potentials $U_{1,2}$, $E_{Z1,2,}$ and $M_{1,2}$, the corresponding Hamiltonian with the tight-binding model is described as:

$$H = -t\sum_{\langle i,j\rangle\sigma} c_{i\sigma}^{\dagger}c_{j\sigma} + t_2\sum_{\langle\langle i,j\rangle\rangle\sigma} e^{-iv_{ij}\phi}c_{i\sigma}^{\dagger}c_{j\sigma} + \sum_{i=1}^{W}\sum_{\sigma}[U_1c_{i\sigma}^{\dagger}c_{i\sigma} + E_{Z1}\mu_i c_{i\sigma}^{\dagger}c_{i\sigma} + M_1c_{i\sigma}^{\dagger}\sigma_{\sigma\sigma}^{z}c_{i\sigma}] + \sum_{i=N_y-W+1}^{N_y}\sum_{\sigma}[U_2c_{i\sigma}^{\dagger}c_{i\sigma} + E_{Z2}\mu_i c_{i\sigma}^{\dagger}c_{i\sigma} + M_2c_{i\sigma}^{\dagger}\sigma_{\sigma\sigma}^{z}c_{i\sigma}] \quad (1)$$

where $c_{i\alpha}^{\dagger}\,(c_{i\alpha})$ are the electronic creation (annihilation) operator with the spin σ $(\sigma = \uparrow\downarrow)$ at site *i*; $\langle i,j\rangle$ and $\langle\langle i,j\rangle\rangle$ run over all the nearest and the next-nearest-neighbor hopping sites. The first term describes the nearest-neighbor coupling of electrons with t = 2.7 eV. The second term denotes the modified Haldane model resulting in the antichiral edge state, which has been experimentally demonstrated [20, 21]. The t_2 and ϕ is set as 0.03 eV and $-\pi/2$, respectively. For the modified Haldane model, $v_{ij} = 1(-1)$ represents the counterclockwise (clockwise) hopping between the sublattice A, while $v_{ij} = -1(1)$ for the sublattice B. The third and last terms are the side potential, including the potential field $U_{1,2}$, the staggered electric potential $E_{Z1,2}$ with $\mu_i = \pm 1$ for A or B sublattice, and the exchange field $M_{1,2}$, which are applied along the boundaries of the nanoribbon. σ_z are the *z* components of 2×2 Pauli matrix for the electron spin. As shown in Fig. 1, the side potential is applied along two boundaries of the zGNRs with the same width $W = 8$. Here we note that the U, E_Z and M are applied separately or jointly along two boundaries of zGNRs according to the different modulation requirements.

For the three-terminal devices, the transmission coefficients (T_{ij}) from lead *i* to lead *j* is calculated by the Non-equilibrium Green's function (NEGF) formalism. In the spin-resolved case, it is expressed as

$$T_{ij}^{\sigma}(E) = Tr[\mathbf{\Gamma}_j^{\sigma}(E)\mathbf{G}^{R,\sigma}(E)\mathbf{\Gamma}_i^{\sigma}(E)\mathbf{G}^{A,\sigma}(E)]$$

2

In Eq. (2), $\mathbf{G}^{R,\sigma}(E)$ and$\mathbf{G}^{A,\sigma}(E)$ are the retarded and advanced Green's function with the spin σ; $\mathbf{\Gamma}_i^{\sigma}(E)$ $(i=1,2,3)$ is the spin-resolved linewidth function of lead *i*, which describes the coupling between the conductor region and lead *i*. The retarded (advanced) Green's function is calculated by the formula below.

$$\mathbf{G}^{R(A),\sigma}(E)=[E_{+(-)}\mathbf{I}-\mathbf{H}_D^{\sigma}-\sum_i \mathbf{\Sigma}_i^{R(A),\sigma}(E)]^{-1}$$

3

In Eq. (3), $E_+=E+i\eta=[E_-]^*$, where and η are the incoming electron energy and an infinitesimal positive number, respectively; $\mathbf{I}$is the identity matrix;$\mathbf{\Sigma}_i^{R,\sigma}(E)=\mathrm{H}_{D,i}\mathbf{g}_i^{R,\sigma}\mathbf{H}_{i,D}$ is the retarded self-energy matrix with $\mathrm{H}_{D,i}$ and $\mathbf{H}_{i,D}$ being the coupling matrix between the conductor and the lead *i*; $\mathbf{g}_i^{R,\sigma}$is the retarded surface Green's function of lead *i*, which can be calculated by using the routine of Lopez-Sancho's iterative method [32].

To investigate the antichiral edge states in zGNRs and understand the electron transport details in the three-terminal device, we plot the local bond current in the leads and conductor region. The energy-dependent local bond current formula between site *i* and *j* reads [33, 34]:

$$J_{ij}^{\sigma}(E)=H_{ji}^{\sigma}G_{ij}^{<,\sigma}(E)-G_{ji}^{<,\sigma}(E)H_{ij}^{\sigma}$$

4

where $\mathbf{G}^{<,\sigma}(E)$ is the lesser Green's function in the energy domain expressed as:

$$\mathbf{G}^{<,\sigma}(E)=-i\mathbf{G}^{R,\sigma}(E)\mathbf{\Gamma}_{\alpha}^{\sigma}(E)\mathbf{G}^{A,\sigma}(E)$$

5

and H_{ij}^{σ} is the relevant matrix element of the conductor's Hamiltonian. It is noted that this formula is related to the local bond current from the incidence of lead α.

3. Results And Analysis

In this section, we mainly study the impact of the side potential on pristine antichiral edge states, and the transport property of the tunable antichiral edge states in the three-terminal device. Note that the widths of the upper and lower potentials are assumed to be the same (W = 8) for convenience in the following discussion, and the main conclusions are still valid when the W becomes different. In addition, to clearly see the band for the edge states, we only present the local profile of the band in the Figures. In the following Figures, the band structures (or the edge states) for spin degeneracy, spin-up and spin-down electrons are highlighted by the black, red and blue curves (or arrows), respectively. Here we note that the U, E_Z and M are applied separately or jointly along two boundaries of zGNRs according to the different

modulation requirements. For example, if we do not show the value of the U, this represents $U_1 = U_2 = 0$, and other cases are similar.

3.1 Five possible types of antichiral edge states

As shown in Fig. 2, the pristine antichiral edge state is obtained based on the modified Haldane model [16] in zGNRs. Figure 2(a) shows the energy band of antichiral edge states, where the edge states propagate in the same direction at two parallel boundaries (Fig. 2(a) inset: the thin black arrows), and the gapless bulk states with counterpropagating modes (Fig. 2(a) inset: the thick black arrows). For the zGNRs-based two-terminal system, if one sets both the leads and conductor as a modified Haldane model, then the edge states can be shown by calculating the local bond current distribution. Figure 2(b) shows the result of the local bond current distribution of the spin-up (down) edge states and spin degeneracy case, which is consistent with the edge state in Fig. 2(a).

Two edge states (spin-up and spin-down modes) both in the upper and lower boundaries of the zGNRs for the pristine antichiral edge states. Thus, we can propose five forms of antichiral edge states by removing the edge modes on the boundary of the zGNRs. As shown in Fig. 3, there is Type-1 when we consider eliminating one edge state in the upper or lower boundary. And there are Type-2, Type-3 and Type-4 when two edge modes are removed from the boundary. For Type-2, the spin-up and spin-down edge states in the upper or lower boundary are removed simultaneously. The Type-3 and Type-4 are obtained by subtracting different and same spin edge states in the upper and lower boundaries, respectively. Similarly, one obtains Type-5 when three edge modes are removed from the boundary of the nanoribbon.

The five types of antichiral edge states have been proposed, and we will show how to obtain these intriguing edge states by manipulating side potential in the next discussion.

3.2 Side potential-tunable antichiral edge states

In this section, we will show how to obtain the five types of antichiral edge states by modulating side potential. As shown in Fig. 1, the side potential is composed of potential field U, staggered potential field E_Z, and exchange field M applied along the boundaries of the zGNRs ($W = 8$). There are two or more cases in each type, but due to the similarity, we only introduce one case in each type.

As shown in Fig. 4(a), the energy band of the Type-1 that spin-up mode in the upper boundary is removed from the pristine antichiral edge states, which can be obtained with $U_1 = 0.2t$ and $M_1 = 0.2t$. From the result of the local bond current distribution (illustration on the left) and the probability distributions (Fig. 4(b) and (c)), one can see that the spin-up edge modes with positive velocity are only localized near the upper boundary of the ribbon, while the spin-down modes with positive velocity are localized on the upper and lower boundaries simultaneously.

The Type-2 is obtained by applying $U_1 = 0.2t$ or $M_1 = 0.2t$, in which the spin-up and spin-down modes both are removed from the upper boundary or lower boundary of the zGNRs. The results of Fig. 5(a) and (b) correspond to $U_1 = 0.2t$ and $M_1 = 0.2t$, respectively. Both the results of Fig. 5(a) and (b) are the same although they appear different. From the result of the local bond current distribution (illustration on the left), one can see that the spin-up and spin-down edge modes with positive velocity are localized near the lower boundary of the ribbon simultaneously.

Similarity, one can obtain the Type-3 (Fig. 6(a)) with applying $M_1 = 0.2t$, $M_2 = 0.2t$, $E_Z = 0.2t$ simultaneously, the Type-4 (Fig. 6(b)) with applying $U_1 = 0.1t$, $U_2 = -0.1t$, $M_1 = -0.1t$, $M_2 = 0.1t$ simultaneously, and the Type-5 (Fig. 6(c)) with applying $U_1 = 0.2t$, $M_2 = 0.2t$, $E_Z = 0.2t$ simultaneously.

By modulating side potential, we have obtained five types of antichiral edge states discussed above, where the U, E_Z and M are applied separately or jointly along two boundaries of zGNRs depending on the different modulation requirements. However, the side potential-tunable mechanism needs to be clarified. In the following, we discuss the independent effect of the U, E_Z and M on the pristine antichiral edge states, and then use their combined effect to explain the formation of novel edge states.

Figure 7 shows the results of the band structure of the zGNRs with $M_1 = 0.2t$ (Fig. 7(a1)), $M_2 = 0.2t$ (Fig. 7(a2)), $U_1 = 0.2t$ (Fig. 7(b1)), $U_2 = 0.2t$ (Fig. 7(b2)), $E_{Z1} = 0.2t$ (Fig. 7(c1)), and $E_{Z2} = 0.2t$ (Fig. 7(c2)). The result of Fig. 7(a1) indicates that the spin-up and spin-down edge modes in the upper boundary are destroyed near Fermi energy when the exchange field is applied along the upper boundary, while the edge modes in lower boundary are not changed. Although the two figures look the same, the result of Fig. 7(a2) is the opposite of Fig. 7(a1). It is noted that the energy band in spin-up edge mode moves upward, but the band in spin-down edge mode moves downward for both Figs. 7(a1) and (a2). Similarly, Figs. 7(b1) and (b2) show the result that upper and lower edge states are eliminated by applying the U_1 and U_2, respectively. And the results of Fig. 7(c1) and (c2) are similar with Fig. (b1) and (b2), but there are some differences between them. The edge modes are destroyed with the band moving upward by applying U. However, the E_{Z1} and E_{Z2} lead to the band of the upper and lower edge states moving upward and downward, respectively. The reason is that both upper and lower boundaries are composed of different lattice atoms, and E_Z is sensitive to the lattice type while U is not.

We have understood the effect on the energy band of edge modes when U, E_Z and M are applied separately along two boundaries of zGNRs based on the detailed analysis above. Next, we take the results of Fig. 4(a) as an example to understand their combined effects. For the pristine antichiral edge states, the energy band of the upper edge states moves upward with applying the U_1 (Fig. 7(b1)). Then, the spin-up band of the upper edge modes continues to move upward with applying the M_1 while the spin-down band moves downward. The lower edge states remained unchanged when U_1 and M_1 are applied along the boundary of the zGNRs. Finally, the result of Fig. 4(a) is obtained.

3.3 Spin/charge current switcher in the three-terminal device

We have obtained the five antichiral edge states by manipulating the side potential. Next, we propose a spin/charge current switcher based on these edge states in a three-terminal system consisting of the zGNRs. As shown in Fig. 8(a), the three-terminal device includes the four parts: lead 1, conductor, lead 2 and lead 3. The currents are incident from lead 1 and finally transmitted into lead 2 and lead 3. Among these parts, the lead 1, lead 2 and lead 3 are set as pristine antichiral edge states, but the conductor with the side potential-tunable antichiral edge modes. Five types of outputs can be achieved by side potential-tunable antichiral edge states in the conductor. Here, we take one case of the Type-3 (Fig. 6(a)) as an example to discuss its output, and other cases are similar. Figures. 8(b) and (c) show the results of transmission and local bond current, respectively. These results indicate that spin-up and spin-down currents are been separated from the output leads when the edge state of the conductor is set as Type-3 (Fig. 2), which corresponds to the result of Fig. 6(a). Both charge and spin currents can also be obtained when the edge state of the conductor is set as Type-1. Thus, the above results show that the three-terminal device proposed is a spin/charge switcher.

4. Conclusions

In summary, based on the pristine antichiral edge states, considering permutation combinations, we propose five types of antichiral edge states. The pristine antichiral edge states have four edge modes, including two spin-up and two spin-down edge modes. There is Type-1 when we consider eliminating one edge mode in the upper or lower boundary. One obtains Type-2, Type-3, and Type-4 when two edge modes are removed from the boundary. Similarly, the Type-5 is obtained when three edge modes are removed from the boundary of the nanoribbon. We obtain these antichiral edge states by modulating the side potential applied on the boundaries of the zGNRs. One can understand the regulatory mechanism by applying separately the U, E_Z and M along two boundaries of zGNRs. The energy band in spin-up edge mode moves upward, but the band in spin-down edge mode moves down when M is applied on the upper or lower boundary. The edge modes are destroyed with the band moving upward by applying U along the boundary of the zGNRs. And with applying the E_Z, the band of the upper and lower edge states moves upward and move down, respectively. Combining their effects on the energy band, we can obtain five antichiral edge states. In addition, we also proposed a perfect spin/charge switcher in the three-terminal device based on the side potential-tunable antichiral edge states. We believe that these results are vital for future spintronics device designs.

References

1. A.K. Geim, Graphene: status and prospects, science 324(5934) (2009) 1530–1534.
2. K.S. Novoselov, L. Colombo, P. Gellert, M. Schwab, K. Kim, A roadmap for graphene, nature 490(7419) (2012) 192–200.

3. V. Gusynin, S. Sharapov, Unconventional integer quantum Hall effect in graphene, Physical review letters 95(14) (2005) 146801.
4. N. Nagaosa, J. Sinova, S. Onoda, A.H. MacDonald, N.P. Ong, Anomalous hall effect, Reviews of modern physics 82(2) (2010) 1539.
5. C. Kramberger, R. Hambach, C. Giorgetti, M. Rümmeli, M. Knupfer, J. Fink, B. Büchner, L. Reining, E. Einarsson, S. Maruyama, Linear plasmon dispersion in single-wall carbon nanotubes and the collective excitation spectrum of graphene, Physical review letters 100(19) (2008) 196803.
6. J. Yan, Y. Zhang, P. Kim, A. Pinczuk, Electric field effect tuning of electron-phonon coupling in graphene, Physical review letters 98(16) (2007) 166802.
7. C.L. Kane, E.J. Mele, Quantum spin Hall effect in graphene, Physical review letters 95(22) (2005) 226801.
8. C.L. Kane, E.J. Mele, Z 2 topological order and the quantum spin Hall effect, Physical review letters 95(14) (2005) 146802.
9. H. Ishida, A. Liebsch, Engineering edge-state currents at the interface between narrow ribbons of two-dimensional topological insulators, Physical Review Research 2(2) (2020) 023242.
10. X.-L. Lü, H. Xie, Spin filters and switchers in topological-insulator junctions, Physical Review Applied 12(6) (2019) 064040.
11. J.-E. Yang, X.-L. Lü, H. Xie, Current propagation behaviors and spin filtering effects in three-terminal topological-insulator junctions, New Journal of Physics 22(10) (2020) 103018.
12. J.-E. Yang, X.-L. Lü, H. Xie, Three-terminal spin/charge current router, Journal of Physics: Condensed Matter 32(32) (2020) 325301.
13. J.-E. Yang, X.-L. Lü, C.-X. Zhang, H. Xie, Topological spin–valley filtering effects based on hybrid silicene-like nanoribbons, New Journal of Physics 22(5) (2020) 053034.
14. X. Zhai, R. Wen, X. Zhou, W. Chen, W. Yan, L.-Y. Gong, Y. Pu, X.a. Li, Valley-mediated and electrically switched bipolar-unipolar transition of the spin-diode effect in heavy group-IV monolayers, Physical Review Applied 11(6) (2019) 064047.
15. J. Zheng, Y. Xiang, C. Li, R. Yuan, F. Chi, Y. Guo, Multichannel Depletion-Type Field-Effect Transistor Based on Ferromagnetic Germanene, Physical Review Applied 16(2) (2021) 024046.
16. E. Colomés, M. Franz, Antichiral edge states in a modified Haldane nanoribbon, Physical Review Letters 120(8) (2018) 086603.
17. D. Bhowmick, P. Sengupta, Antichiral edge states in Heisenberg ferromagnet on a honeycomb lattice, Physical Review B 101(19) (2020) 195133.
18. J. Chen, W. Liang, Z.-Y. Li, Antichiral one-way edge states in a gyromagnetic photonic crystal, Physical Review B 101(21) (2020) 214102.
19. S. Mandal, R. Ge, T.C.H. Liew, Antichiral edge states in an exciton polariton strip, Physical Review B 99(11) (2019) 115423.

20. Y. Yang, D. Zhu, Z. Hang, Y. Chong, Observation of antichiral edge states in a circuit lattice, Science China Physics, Mechanics & Astronomy 64(5) (2021) 1–7.
21. P. Zhou, G.-G. Liu, Y. Yang, Y.-H. Hu, S. Ma, H. Xue, Q. Wang, L. Deng, B. Zhang, Observation of photonic antichiral edge states, Physical Review Letters 125(26) (2020) 263603.
22. X.-L. Lü, H. Xie, Bipolar and unipolar valley filter effects in graphene-based P/N junction, New Journal of Physics 22(7) (2020) 073003.
23. M. Vila, N.T. Hung, S. Roche, R. Saito, Tunable circular dichroism and valley polarization in the modified Haldane model, Physical Review B 99(16) (2019) 161404.
24. M. Mannaï, S. Haddad, Strain tuned topology in the Haldane and the modified Haldane models, Journal of Physics: Condensed Matter 32(22) (2020) 225501.
25. J. Mei, L. Shao, H. Xu, X. Zhu, N. Xu, Photomodulated edge states and multiterminal transport in silicenelike nanoribbons, Physical Review B 99(4) (2019) 045444.
26. W. Apel, G. Pal, L. Schweitzer, Energy gap in graphene nanoribbons with structured external electric potentials, Physical Review B 83(12) (2011) 125431.
27. S. Bhowmick, V.B. Shenoy, Weber-Fechner type nonlinear behavior in zigzag edge graphene nanoribbons, Physical Review B 82(15) (2010) 155448.
28. C.-H. Chiu, C.-S. Chu, Effects of edge potential on an armchair-graphene open boundary and nanoribbons, Physical Review B 85(15) (2012) 155444.
29. K.W. Lee, C.E. Lee, Topological confinement effects of electron-electron interactions in biased zigzag-edge bilayer graphene nanoribbons, Physical Review B 97(11) (2018) 115106.
30. W.-T. Lu, Q.-F. Sun, Y.-F. Li, H.-Y. Tian, Spin-valley polarized edge states and quantum anomalous Hall states controlled by side potential in two-dimensional honeycomb lattices, Physical Review B 104(19) (2021) 195419.
31. W.-T. Lu, Q.-F. Sun, H.-Y. Tian, B.-H. Zhou, H.-M. Liu, Band bending and zero-conductance resonances controlled by edge electric fields in zigzag silicene nanoribbons, Physical Review B 102(12) (2020) 125426.
32. M.L. Sancho, J.L. Sancho, J. Rubio, Quick iterative scheme for the calculation of transfer matrices: application to Mo (100), Journal of Physics F: Metal Physics 14(5) (1984) 1205.
33. S.R. Power, M.R. Thomsen, A.-P. Jauho, T.G. Pedersen, Electron trajectories and magnetotransport in nanopatterned graphene under commensurability conditions, Physical Review B 96(7) (2017) 075425.
34. T. Stegmann, N. Szpak, Current splitting and valley polarization in elastically deformed graphene, 2D Materials 6(1) (2018) 015024.

Figures

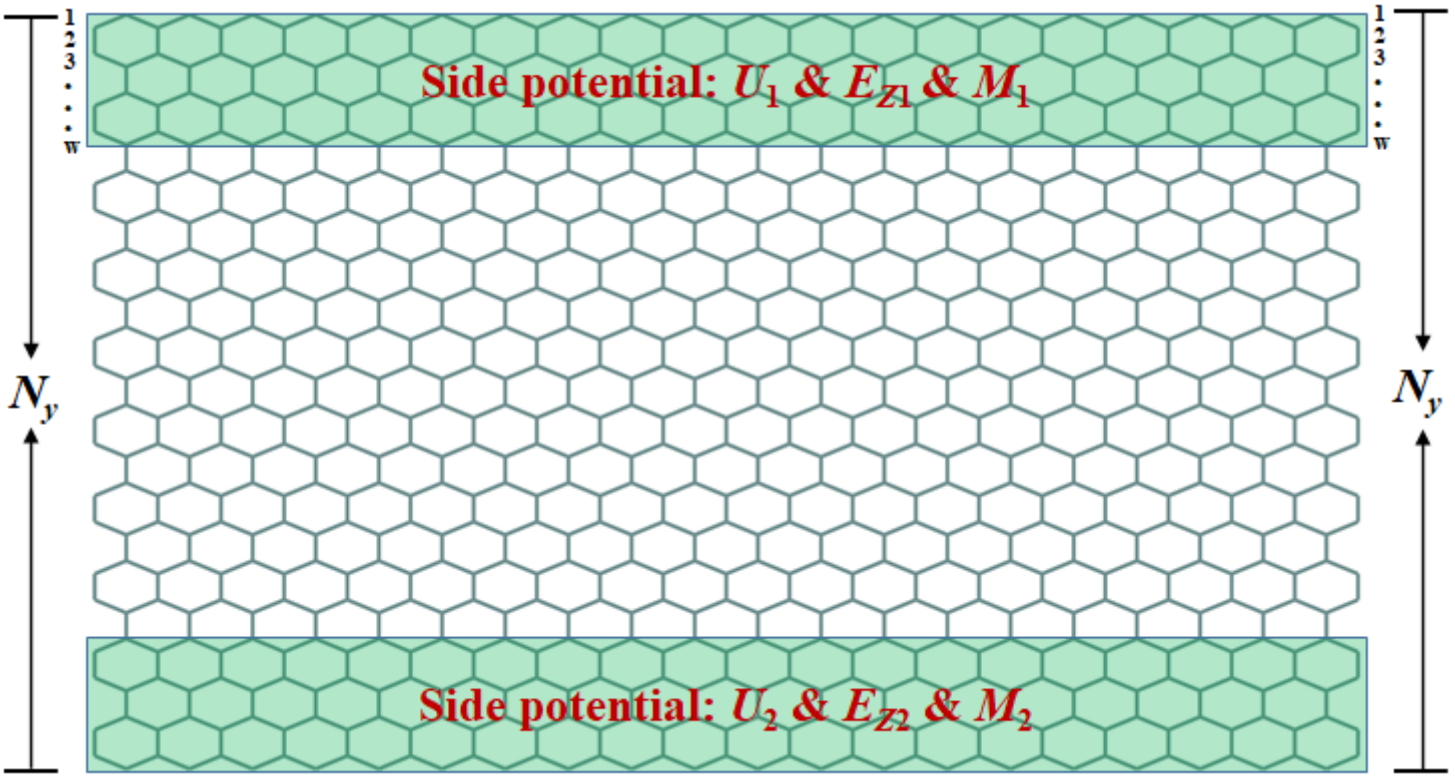

Figure 1

Schematic plot of the zGNRs with potential field $U_{1,2}$, staggered potential field $E_{Z1,2}$, and exchange field $M_{1,2}$ along the boundaries. The ribbon width N_y is defined by the number of carbon atoms along the width, and $W = 8$ describes the width of the side potentials.

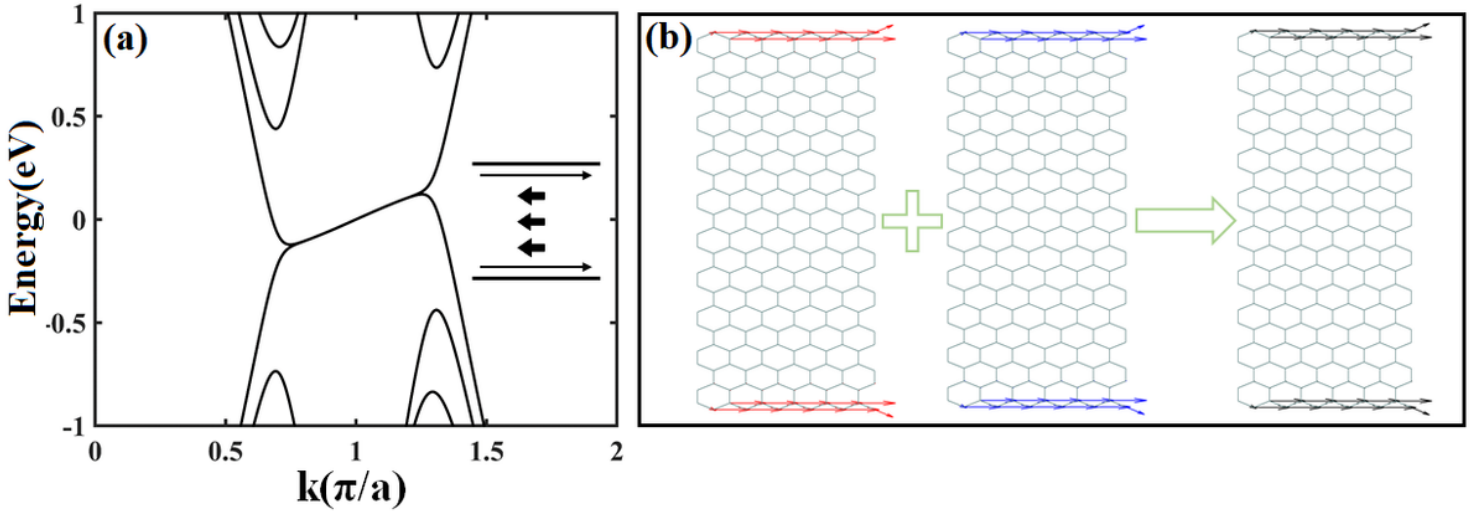

Figure 2

(a) The band structure for pristine antichiral edge states. Inset: schematic diagram of corresponding edge states. (b) The local bond current distribution ($E = 0.03$ eV) for the pristine antichiral edge states. The

black band (arrows) denote the spin degeneracy case, and the red (blue) arrows in the figures denote the spin-up (down) case. The other fixed parameters in all the cases are: $N_y = 40$, $W = 8$.

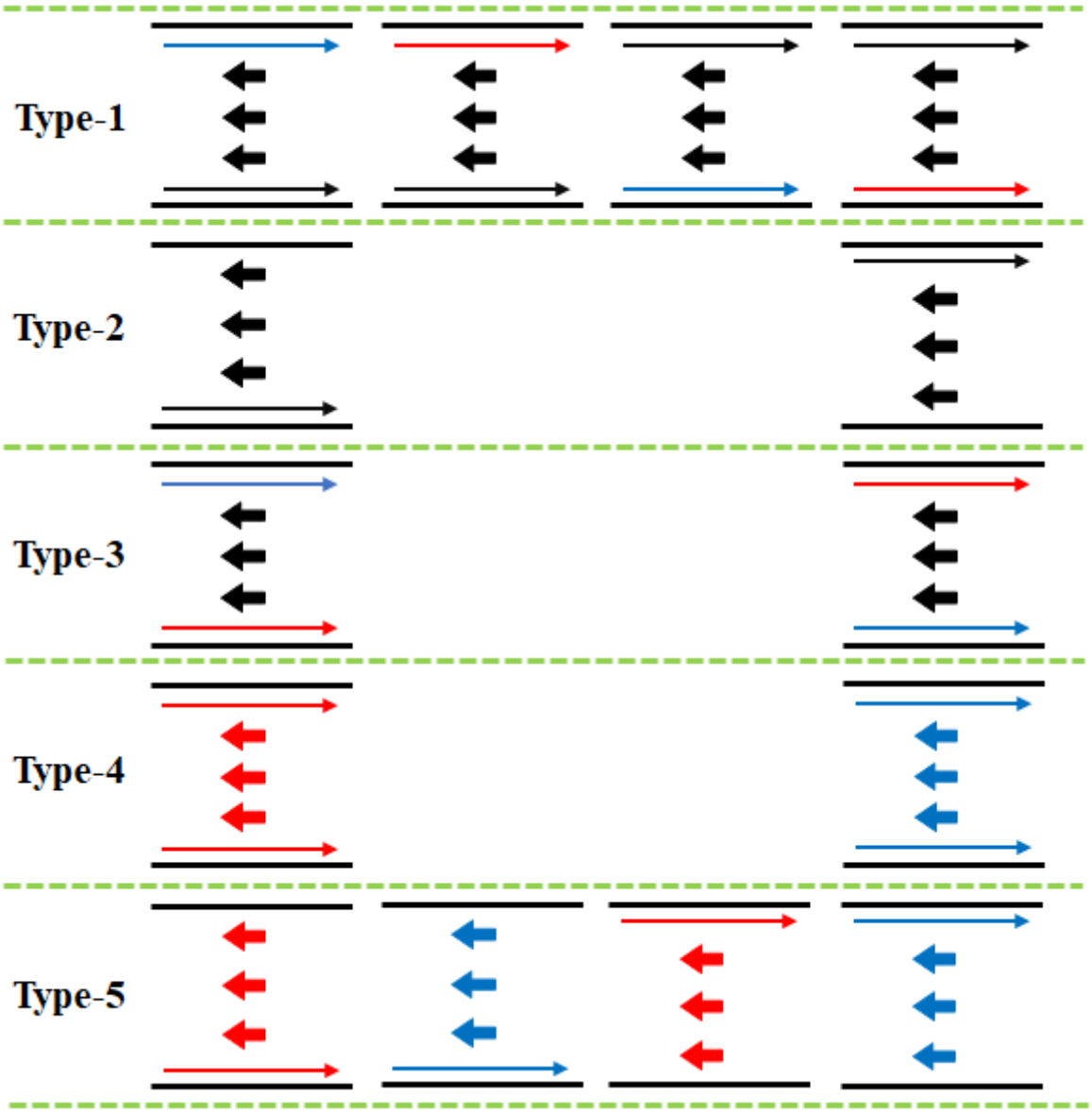

Figure 3

Schematic diagram of the five possible types of the antichiral edge states. The black arrows denote the spin degeneracy case, and the red (blue) arrows denote the spin-up (down) case.

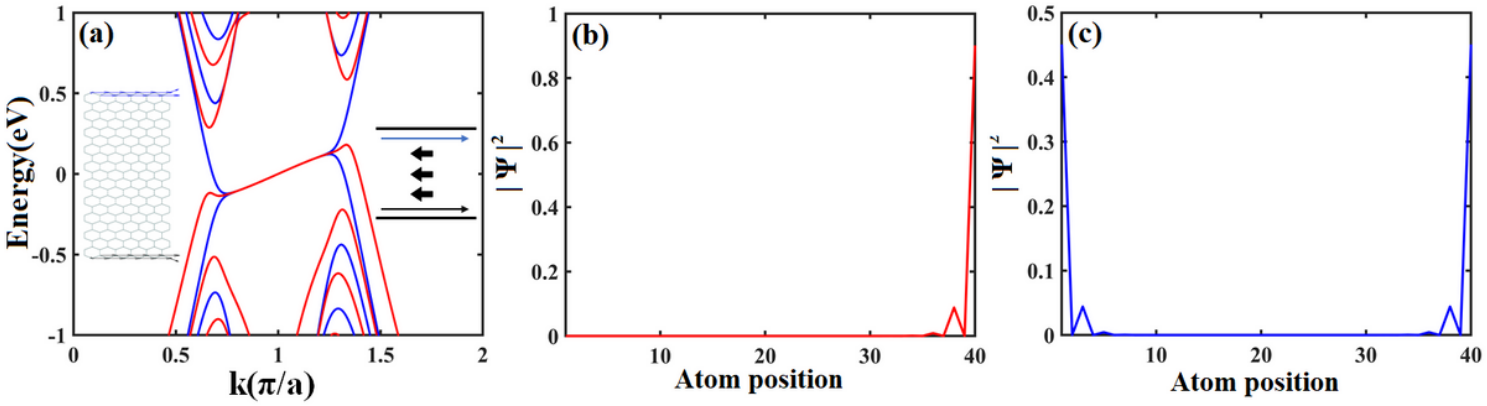

Figure 4

(a) The band structure for one case of the Type-1 with $U_1 = 0.2t$ and $M_1 = 0.2t$ along the boundaries. Inset: local current distribution (left; $E = 0.03$ eV) and schematic diagram of corresponding edge states (right). (b) Corresponding probability distributions of the edge states near the Fermi energy. The black band (arrows) denote the spin degeneracy case, and the red (blue) arrows in the figures denote the spin-up (down) case. Other fixed parameters are same as Fig. 2.

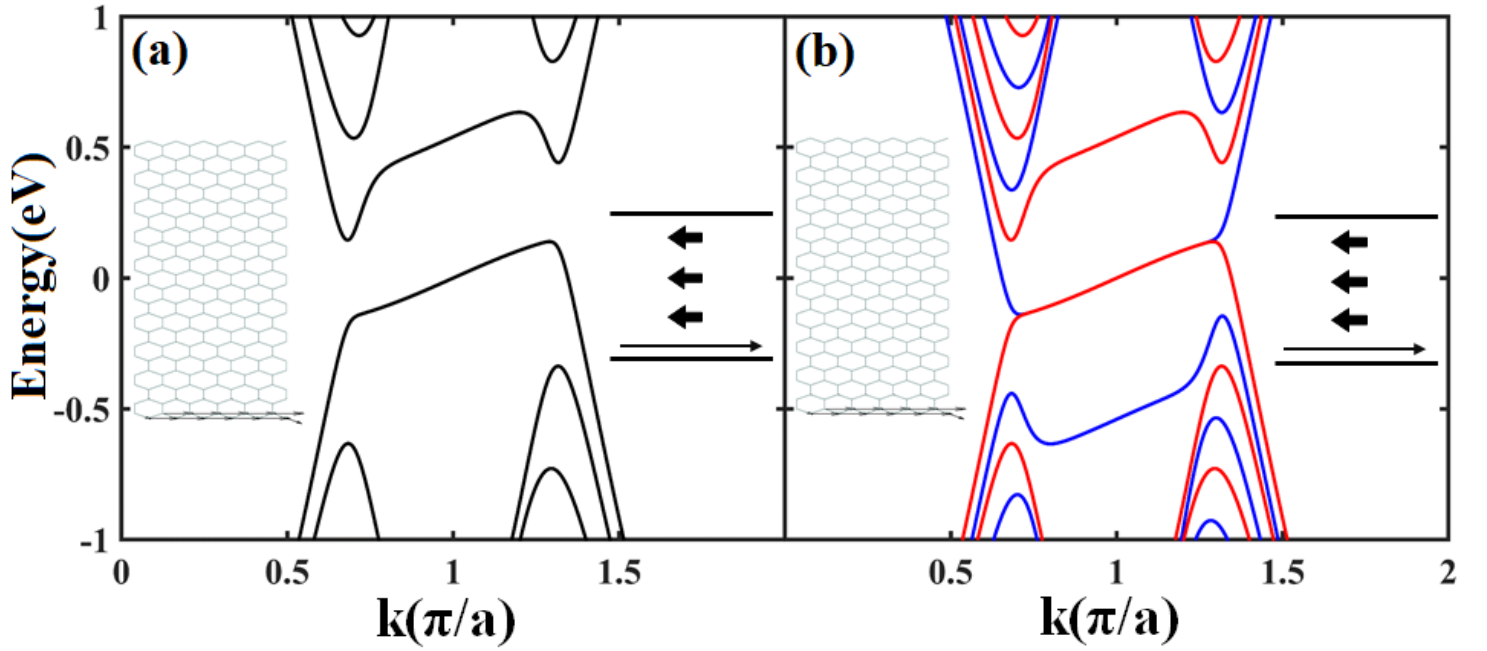

Figure 5

The band structure for one case of the Type-2 with (a) $U_1 = 0.2t$; (b) $M_1 = 0.2t$ along the boundaries. Inset: local current distribution (left; $E = 0.03$ eV) and schematic diagram of corresponding edge states (right). Other fixed parameters are same as Fig. 2.

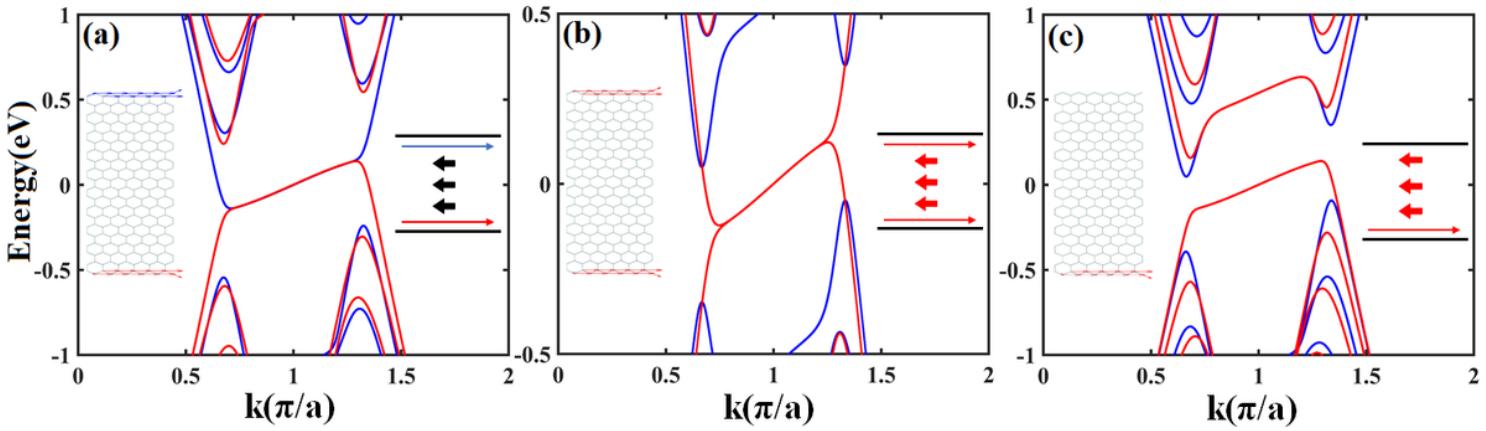

Figure 6

The band structure for one case of (a) the Type-3 with $M_1 = 0.2t$, $M_2 = 0.2t$, $E_Z = 0.2t$, (b) the Type-4 with $U_1 = 0.1t$, $U_2 = -0.1t$, $M_1 = -0.1t$, $M_2 = 0.1t$, (c) the Type-4 with $U_1 = 0.2t$, $M_2 = 0.2t$, $E_Z = 0.2t$. Inset: local bond current distribution (left; $E = 0.03$ eV) and schematic diagram of corresponding edge states (right). Other fixed parameters are same as Fig. 2.

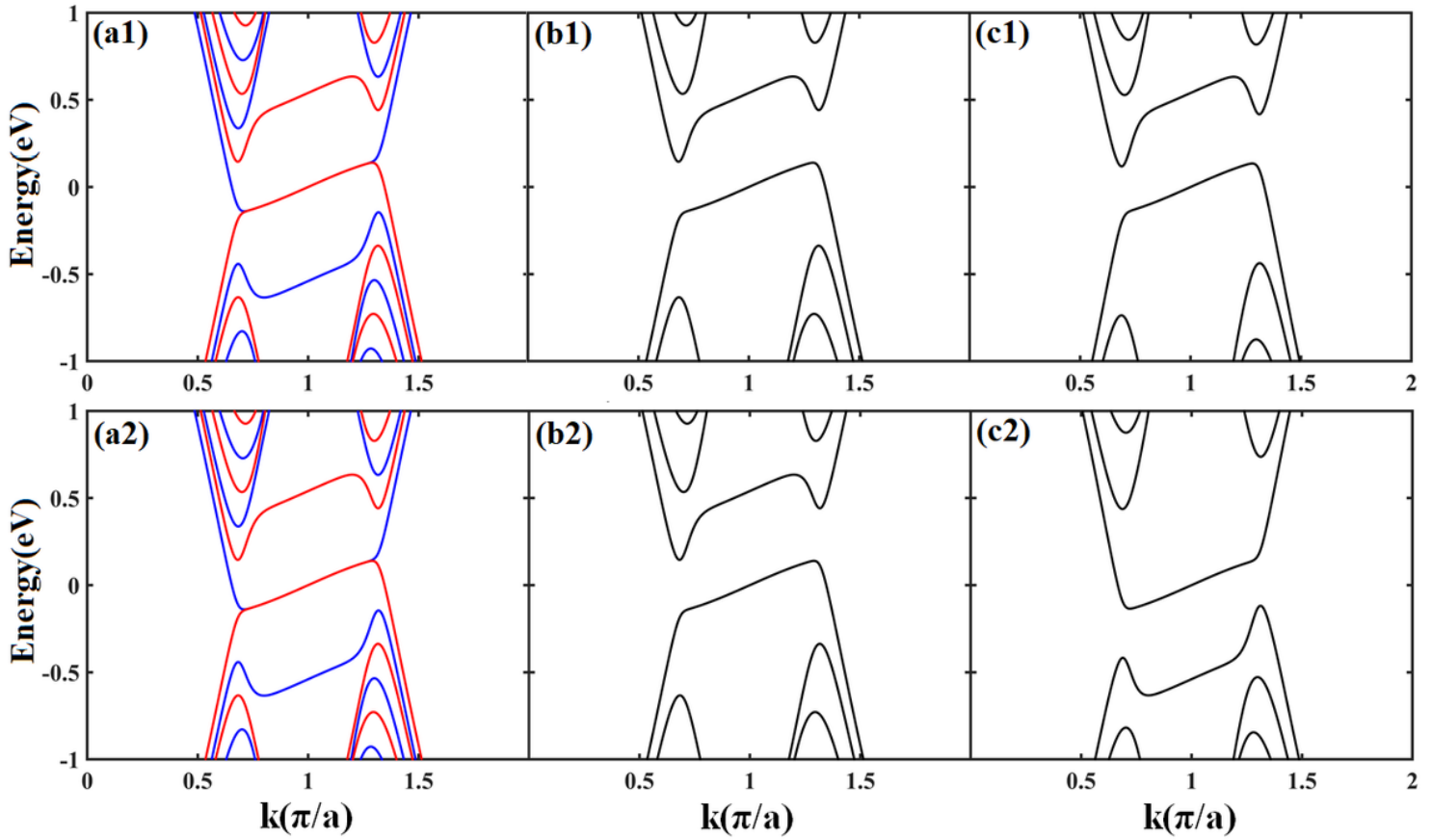

Figure 7

The effect of different side potential applied on boundaries of the zGNRs on the energy band. (a1) M_1 = 0.2t, (a2) M_2 = 0.2t, (b1) U_1 = 0.2t, (b2) U_2 = 0.2t, (c1) E_{Z1} = 0.2t, (c2) E_{Z2} = 0.2t.

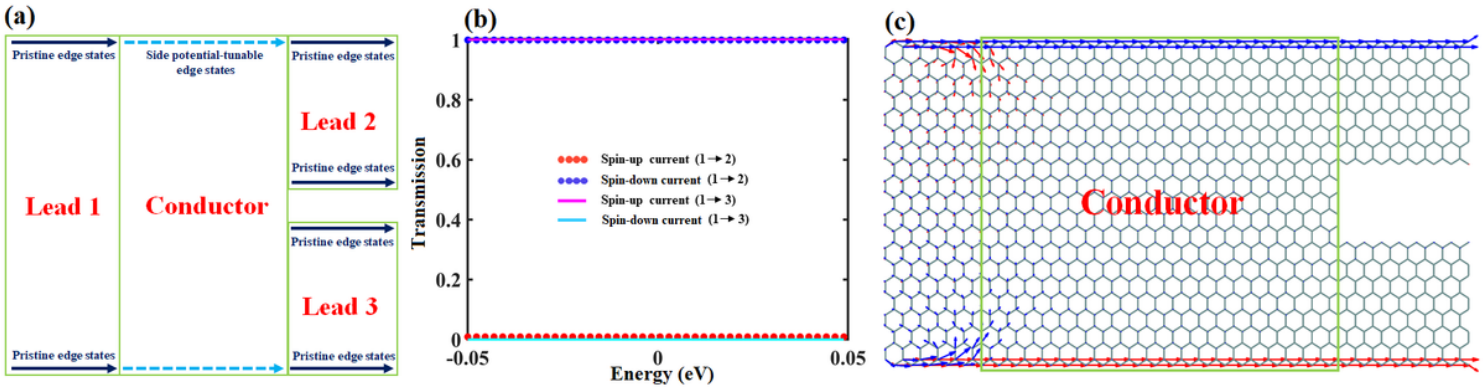

Figure 8

(a) Schematic of the three-terminal spin/charge current switcher. All leads are set as pristine antichiral edge states, and the conductor is applied on side potential-tunable edge states. (b) Transmission spectrum for Type-3. (c) Corresponding local bond current distribution (E = 0.03 eV).